L-edge x-ray-absorption systematics of the noble metals Rh, Pd, and Ag and the main-group metals In and Sn: A study of the unoccupied density of states in $4d$ elements

T. K. Sham
Chemistry Department, Brookhaven National Laboratory, Upton, New York 11973
(Received 25 July 1984; revised manuscript received 15 October 1984)

X-ray-absorption L-edge spectra have been obtained for the noble metals Rh, Pd, and Ag and the main-group metals In and Sn. The systematics derived from these spectra reveal that (a) the x-ray-absorption near-edge structure (XANES) is primarily related to the density of states in these systems, (b) the energy distribution of the states above the Fermi level in noble metals is qualitatively consistent with the general band-theory description and semiquantitatively in agreement with the single-particle theory of Müller, Jensen, and Wilkins, and (c) the $L_{\mathrm{II,III}}$ "white-line" intensity ratio depends on the distribution of the $d_{5/2}$ and $d_{3/2}$ population above the Fermi level and this distribution deviates significantly from the statistical distribution when the d band of the metal is nearly full. The applicability of XANES in the investigation of the charge-distribution systematics in $4d$ elements is discussed.

I. INTRODUCTION

X-ray-absorption spectroscopy (XAS) of core levels has recently found increasing application[1] in the probing of the structure, electronic properties, and dynamic behavior of a large variety of materials through both experimental and theoretical advances. This development is mainly due to the advancement of synchrotron technology. In this paper a systematic study of the L-edge absorption spectra of the metallic elements Rh, Pd, Ag, In, and $_{50}$Sn is presented. The applicability of L-edge spectra in probing the electronic properties of these systems is discussed.

In a core-level absorption spectrum, the behavior of the absorption coefficient μ of an element is studied as a function of photon energy. The absorption coefficient usually increases dramatically (jumps) when the photon energy approaches[2] the binding energy of a core level. For elements with low atomic numbers, the binding energy of the core levels can be reached with photons in the vacuum-ultraviolet or soft-x-ray region, while heavier elements have core levels that can only be reached with x rays. Synchrotron radiation from electron storage rings blurs the distinction and provides a continuous photon-energy spectrum from which photons at a desirable wavelength region can be extracted with proper optics for XAS measurements.[3–6] The absorption coefficient near and above an absorption edge is of particular concern in x-ray-absorption spectroscopy.[7,8]

There are several parameters that are relevant to the interpretation of the edge structure. One is the position of the edge jump E_0. For metallic systems, this is often taken as the point of inflection of the rising absorption edge. The other is the photoelectron threshold E_{th}, which is the minimum energy required to excite the core electron to the vacuum level. For metallic systems with partially filled d bands at the Fermi level, the $L_{\mathrm{II,III}}$-edge jump is the Fermi level (E_F), while in nonmetallic systems the edge jump is merely the rising edge of a well-defined transition, and the peak position E_A is of importance. The separation between E_A and the threshold can be as much as 20 eV in the latter case.[9] Bound-to-bound transitions can occur within this region, resulting in well-defined absorption features[7–10] (sometimes called "white lines"). In the region within $\sim$50 eV above the ionization threshold, there exist bound-to-quasibound—transition features that are sometimes called shape resonances in molecules, and transitions to higher bands or excitons in condensed matter.[11] Beyond this region is the well-known extended x-ray-absorption fine structure (EXAFS).[12] The aforementioned first $\sim$50-eV region is often referred to as the x-ray-absorption near-edge structure (XANES),[1] or near-edge x-ray-absorption fine structure (NEXAFS).[13]

Although standard procedures to extract local structure (bond lengths, coordination numbers, and perhaps bond angles) and dynamic behavior (Debye-Waller factor) from EXAFS have been well established in the last decade,[11–14] the development of the corresponding procedures in the data analysis of XANES has been relatively recent.[1] While XANES spectroscopy permits one to obtain information complementary to EXAFS, such as the electronic properties of the unoccupied states, and, under favorable conditions, even bond lengths,[13] the analysis is far more complicated than that of EXAFS in that the underlying principles for the analysis of XANES depend upon the nature of the class of materials[13,15–37] under investigation. It is, however, not the intention of this paper to compare all the approaches to the interpretation of XANES; rather, we want to report the L-edge systematics of some $4d$ elements and discuss the results on the basis of the conventional band-structure description as well as a single-particle calculation recently reported by Müller, Jensen, and Wilkins.[17]

The systems, Rh, Pd, Ag ($4d$ noble metals), Sn, and In (polyvalent metals) were selected with several objectives in

mind. First, it is desirable to substantiate that near-edge absorption (XANES) is related to the density of states[35] (DOS) with a series of elements, of which the filling of the valence states ($4d$, $5s$, and $5p$) across the period is well understood. Second, it is very interesting to investigate experimentally the distribution of the unoccupied states, particularly the d bands, as well as states with higher angular momentum above the Fermi level across the d period in similar structural environments (Rh, Pd, and Ag are all fcc noble metals while In and Sn are main-group metals with similar structure), and to compare the results with theoretical calculations. Any discrepancy can be discussed on the basis of final-state effects. Third, the spin-orbit interaction is also a subject for investigation. Finally, the sensitivity of the absorption features (white lines) to the distribution of unoccupied states at and above the Fermi level in metallic systems is of great interest since this technique could prove valuable for studying charge redistribution and the reactivity of these states upon compound formation. This last consideration leads to the application of the XANES technique to the investigation of a series of $4d$ compounds, Pd, $PdCl_2$, and $PdAl_3$. The results of this study are reported in a second paper (henceforth denoted II) that immediately follows.

This paper is organized as follows: In Sec. II the relationship between L-edge—absorption XANES and the distribution of the density of states is discussed in terms of a single-particle (one-electron) picture. The experimental details are given in Sec. III. Section IV is divided into two subsections for two series of materials: Rh, Pd, and Ag; and In and Sn. Overall L-edge—absorption systematics and other factors not considered in the DOS and single-particle approach are discussed in the summary and conclusions, given in Sec. V. L-edge absorption of elements at the end of the period having rare-gas configurations are considered in a forthcoming paper in which the L-edge—absorption spectra of CsI in the solid state and in solution are discussed in detail.

II. L-EDGE SPECTRA AND THE DISTRIBUTION OF THE DENSITY OF STATES: ONE-ELECTRON PICTURE

The L-edge XANES are often of particular interest in the study of electronic properties of materials because there are three different initial states, $2s$ ($L_{\rm I}$), $2p_{1/2}$ ($L_{\rm II}$), and $2p_{3/2}$ ($L_{\rm III}$), that may be coupled to final states of p, s, and d character, respectively. This results in distinctly symmetry-dependent features at the absorption edges. The relationship between XANES and the density of states in noble metals is illustrated in Fig. 1; the photoemission process which probes the occupied states is also shown for comparison.

Figure 1 shows the schematics of the distribution of the density of states, denoted $N(E)$ near the Fermi level for the noble metals at the end of the d period. The DOS is conveniently divided into a d band and a very broad free-electron-like sp band; the d band moves down in energy and narrows as it becomes filled across the $4d$ period. XANES features shown on the upper left-hand side of the figure arise from dipole transitions from the core levels to the unoccupied states above the Fermi level. In photo-

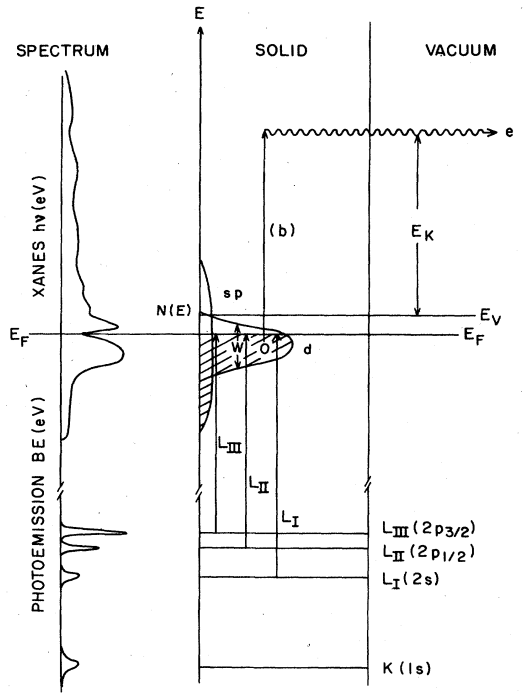

FIG. 1. Schematic diagram illustrating the photoabsorption and photoemission processes for noble metals and the resulting XANES and photoemission spectra; E_F is the Fermi level, E_V is the vacuum level, E_K is the kinetic energy of the photoelectron, and $N(E)$ is the density of states, which shows a characteristic narrow d band and a free-electron-like sp band; in noble metals the d band becomes filled at the d^{10} configuration (Cu, Ag, and Au) and drops below the Fermi level. See text.

emission studies with fixed photon energy, core levels can only be excited by photons with energy greater than the binding energy of the core electrons. An analysis of the electron kinetic energy E_K would give a spectrum shown on the lower left-hand side of the figure, in which each peak corresponds to a well-defined occupied state in the atom. It must be noted that while XANES probes the unoccupied states, and is a one-step process, photoemission of solids probes the occupied states and can be regarded as a three-step process in which the photoelectron is excited into a high-energy state in the solid, leaving a hole behind [process (b) in Fig. 1], then travels to the surface, and subsequently leaves the solid and is detected. Any structure in the final-state wave function can manifest itself in photon-energy-dependent photoemission experiments (such as angle-resolved photoemission spectroscopy).

The one-electron picture (single-particle transition model) assumes that only one core electron is excited to an unoccupied state of the system (gaseous molecules or solids) upon the absorption of one photon. The passive electrons (electrons not directly excited by the photon absorbed) remain frozen upon excitation. Let us for the moment assume that many-body correlation effects are negligible for metallic systems. We can then analyze the

XANES features in terms of the dipole-transition matrix element, the ground-state partial density of states (PDOS), and final-state broadening.[17] This approach has been well documented. For example, Brown,[11] and Brown, Peierls, and Stern,[16] have discussed the XANES structure on the basis of the single-particle approximation. More recently, Matheiss and Dietz[19] reported relativistic calculations for the interpretation of XANES of Pt and Au. Grunes *et al.* have studied the $3d$ transition metals and oxides.[22,23] Horsley,[30] using the $X\alpha$ scattered-wave ($X\alpha$ SW) technique, has deduced the number of d holes in a series of Pt and Ir compounds from their XANES spectra, and has also shown that the difference in the d-orbital occupancies between different compounds should be fairly accurately measured by the difference in the areas of the white lines. Kostroun *et al.*[35] have studied the K-edge—absorption systematics of $4d$ metals. Balzaratti *et al.*[36] have shown that, for titanium metal and its carbides and nitrides, the local partial density of states at the metal site is responsible for the observed XANES.

Quantitative information such as the distribution and the number of d vacancies in a metal can be obtained from the XANES data, in principle, if the transition matrix element $M_{if}=\langle\Psi_i\,|\,r\,|\,\Psi_f\rangle$ in Eq. (1) is evaluated. We write

$$\mu(h\nu)\propto\sum_f|\langle\Psi_i\,|\,r\,|\,\Psi_f\rangle|^2 n_f\ . \tag{1}$$

In Eq. (1), μ is the absorption coefficient in cm^{-1}, Ψ_i is the initial-state wave function, and Ψ_f is the final-state wave function. Ψ_f is an energy-band state in metals and a molecular orbital in metal complexes, and n_f is the number of vacancies of the final state. The observed spectral intensity A (area under the peak arising from the dipole transition) can be expressed as

$$A=\int\mu(E)dE=\frac{2n_0\pi^2e^2h}{mc}f_{if}n_f\ , \tag{2}$$

where n_0 is the number of atoms in unit volume, m is the mass of the electron, c is the speed of light, and f_{if} is the oscillator strength,

$$f_{if}=(2m\omega_{if}/h)\,|\langle\Psi_i\,|\,r\,|\,\Psi_f\rangle|^2\ . \tag{3}$$

The initial-state wave function in Eq. (3) is always atomiclike regardless of the material studied; the final-state wave function, however, can be very variable compared with the atomic wave functions, depending on the material as well as the energy region under investigation (that is, it depends on whether or not the region is in the vicinity of the threshold or well above the threshold).

In metallic systems, the Ψ_f's are the dispersive and delocalized-band-state wave functions, $\Psi_{\mathbf{k},n}$, which are usually labeled with the reduced wave vector $\mathbf{k}$ and band index n, and the theoretical absorption spectrum is given by

$$\mu(h\nu)\propto\sum_{\mathbf{k},n}|\langle\Psi_i\,|\,r\,|\,\Psi_{\mathbf{k},n}\rangle|^2\delta(h\nu-E_{\mathbf{k},n})n_l(h\nu)\ , \tag{4}$$

where $n_l(h\nu)$ is a partial density of states; $\langle\Psi\,|\,r$ in $\mu(h\nu)$ acts as an operator which projects out the $l=2$ and 0 components of the band states in the case of $L_{\mathrm{II,III}}$ edges, and the $l=1$ component in the case of L_{I} and K edges.

For photon energy well above the threshold ($h\nu-E_0\geq 100$ eV), the absorption is in the EXAFS region, where an electron scattered by the environment interferes with the outgoing electron wave, and the absorption coefficient may be given by[6]

$$\mu(h\nu)\propto|\langle\Psi_i\,|\,r\,|\,\Psi_f'+\Psi_{\mathrm{sc}}\rangle|^2\ , \tag{5}$$

where Ψ_f' is the outgoing photoelectron wave and Ψ_{sc} is the backscattered photoelectron wave. Based on a plane-wave approximation,[12] the conventional EXAFS function $\chi(k)=(\mu-\mu_0)/\mu_0$, where μ_0 is the smooth atomic absorption coefficient, can be expressed (for K edge and random sample, for example) as

$$\chi(k)=\sum_i-\frac{|f(k,\pi)|N_i}{kR_i^2}\exp(-2\sigma_i^2k^2)\times\sin[2kR_i+\phi(k)]\ , \tag{6}$$

where N_i is the number of identical neighboring atoms at a distance R_i with a Debye-Waller factor σ_i, $\phi(k)$ is the phase function, and $f(k,\pi)$ is the backscattering amplitude of the neighboring atom.

It is interesting to note that an x-ray-absorption spectrum has been conventionally divided in two regions based on the formalism applied in the analysis. This approach is more of a matter of convenience than necessity. Attempts to unify the analysis for the two regions are relatively lacking, although they may be considered equivalent on the basis of recent cluster[15] and band[16] calculations that take into account the multiple-scattering effect, which is the strongest in the near-edge region. On the other hand, Müller and Schaich[18] recently proposed a single-scattering formalism that is applicable to these situations.

Returning to Eqs. (1)—(4), it becomes apparent that a successful quantitative analysis of XANES relies on the construction of one-electron initial- and final-state wave functions. Müller *et al.*[17] have recently calculated the x-ray-absorption spectra of a large number of metallic elements using a linearized version[38] of the augmented-plane-wave (APW) method to handle the extended energy range (100 eV above threshold). Despite the neglect of the core-hole effect, their calculations are in good agreement with a large number of XANES structures of metals. In Sec. IV we first make qualitative comparison of the XANES spectra with ground-state band calculations. This is followed by quantitative comparison of our data with the theoretical spectra.[17]

Several factors were omitted in the single-particle formalism. They are relaxation and multielectron processes introduced by the creation and subsequent decay of the core hole and multiplet splittings for systems that have an open valence shell. These are well-known phenomena in photoelectron spectroscopy (PES).[39] In conventional PES studies with Al and Mg $K\alpha$ x rays, the measured binding energy is always less than the calculated one-electron binding energy as a result of final-state screening (relaxation), while the multielectron effect (due to strong electron correlation) leads to shake-up and shake-off processes,

and, in some cases, the disappearance of the one-electron spectrum.[40–44] Although analogous situations are expected to exist in the XANES spectrum, the situation requires considerations not encountered in PES: First, a non-free-electron-like state (bound or quasibound state) is directly participating in the absorption process; second, the energy of the excitation photons, instead of being well above the threshold as in the case of x-ray photoelectron spectroscopy (XPS) studies, is in the vicinity of the threshold. Third, these transitions are modulated by the partial density of states. The influence of the final-state relaxation and multielectron effects in the XANES region of these metallic systems is discussed further in Sec. V.

III. EXPERIMENTAL DETAILS

All the metal samples were prepared as free-standing thin foils or evaporated films on Kapton substrates. The free-standing foils were rolled from bulk metal to a thickness of 0.0001 in. and were subsequently annealed under vacuum at 500 °C in a glass capsule which also contained a piece of rare-earth metal (Nd metal). The rare-earth metal (which was not in contact with the foils) was used as a getter to clean the foils. Separate samples were prepared for Rh, Pd, Ag, and Sn by evaporation. The evaporated films have a coverage of $\sim 1\ \mu g/cm^2$. All the L-edge x-ray-absorption spectra were recorded at ambient temperature in a transmission mode at the Stanford Synchrotron Radiation Laboratory (SSRL) using the focused beam line (II-3). A Si(111) double-crystal monochromator was used. Samples were placed in a metal container filled with dry helium to reduce air absorption. Since the L edges of interest are at very low energy by typical EXAFS considerations, helium was used in the first ionization chamber to reduce absorption by I_0 monitor, while N_2 was used in the second ionization chamber. At these energies (3—5 keV), higher-order radiation is a problem (the mirror cutoff is at ~ 9.5 keV). Their presence would lead to errors in the evaluation of the absorption coefficient and decrease the signal-to-noise ratio. This constitutes part of the so-called thickness effect.[45] This problem is usually dealt with by detuning the monochromator to ~ 30—50% of its maximum through-put. This procedure works well in minimizing the higher-order contribution to the absorption spectrum. The pinhole effect that may exist in the evaporated samples is eliminated by folding the films at least once. K-edge spectra of Pd and Rh have also been obtained at beamline II-2 for comparison with the L_I-edge data. At least two spectra were taken for each sample, sometimes at different fills (electrons in the storage ring need to be refilled periodically) to ensure reproducibility and glitch-free data. I_0 and I (I_0 is the monitor of the incident photon flux and I is the transmitted flux) were collected at separate channels so that both sets of data could be examined separately.

Absorption spectra are plotted with the absorption coefficient, μt, being the ordinate, the photon energy, $h\nu$, the abscissa. The transmitted intensity I and the absorption coefficient are related by

$$\ln(I_0/I)=\mu(E)t\ , \tag{7a}$$

where μ is the linear absorption coefficient of the sample, and t the sample thickness. For better identifying maxima in the spectra, Eq. (7a) is often differentiated to give

$$\frac{d[\ln(I_0/I)]}{dE}=\frac{\partial\mu(E)t}{\partial E}\ . \tag{7b}$$

IV. RESULTS AND DISCUSSION

A. L-edge spectra of Rh, Pd, and Ag

The L-edge spectra of Rh are shown in Fig. 2 for all the L levels (L_I, L_{II}, and L_{III}), plus the first derivative of the Rh L_{III} edge. The L-edge spectra of Pd and Ag are shown in Fig. 3. Several interesting features are immediately noted. First, while both Rh and Pd metals exhibit intense resonance (white lines) at the L_{II} and L_{III} edges, no white line is seen at the Ag L_{II} and L_{III} edges. Second, no white line is observed at any of the L_I edges. Third, despite the drastic difference in the L_{II},L_{III}-edge white-line resonance intensity, the oscillatory behavior of the absorption coefficient above the white line is almost identical in all three metals. Fourth, the relative intensity between the L_{III} and L_{II} white lines is smaller in Rh than in Pd. Finally, the normalized $L_{II,III}$ white-line intensity and shape also appear to be different among these elements. In discussions given below, these observations are first interpreted qualitatively on the basis of one-electron ground-state band-structure calculations by Moruzzi, Gelatt, and Williams (MGW).[46] Their calculations provide information about the density of states of the unoccupied levels up to 10 eV above the Fermi level. After that, quantitative assignments of the L-edge features are made on the basis of the single-particle calculation of the absorption spectrum of these metals by Müller *et al.*[17] up to as much as 100 eV above the edge (XANES approach). The effect of spin-orbit interactions seen in the L-edge white lines is also discussed. Total d-band widths for these metals extracted from previously reported photo-

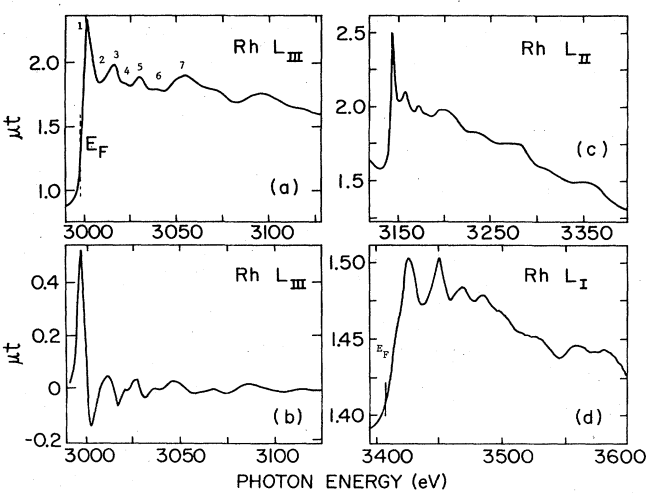

FIG. 2. L-edge—absorption spectra of Rh metal: (a) L_{III} edge with E_F pinned at the point of inflection; (b) first derivative of the Rh L_{III} edge, and the first maximum pins the Fermi level; (c) L_{II} edge; (d) L_I edge.

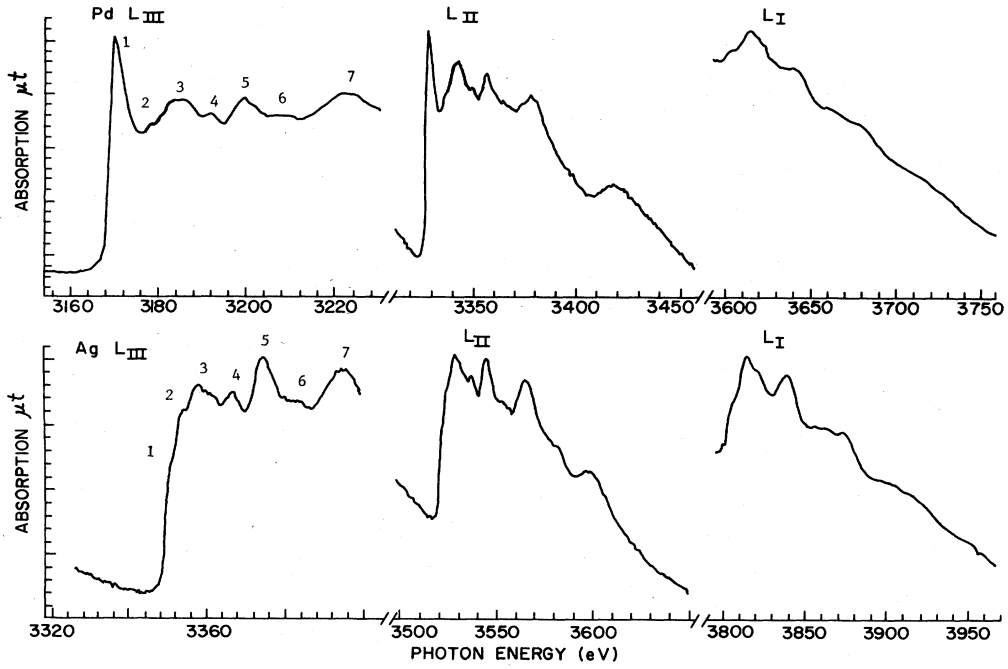

FIG. 3. L-edge—absorption spectra of Pd and Ag metals; the labeled peaks show the similarity in the oscillatory behavior of the L_{III} absorption coefficients between Pd and Ag. [These spectra have better resolution than those reported by L. Pratt, Phys. Rev. **54**, 99 (1938).] Similar patterns can also be seen in the L_{II}- and L_I-edge spectra. The peak positions are listed in Table I.

emission[47] and XANES data reported here are used for comparison with calculations in order to substantiate that the origin of the L-edge—absorption XANES is indeed a density-of-states effect, and that the XANES technique complements photoemission. A comparison between L_I and K spectra is also made for these metals. Finally, the same set of data is analyzed using the EXAFS approach at the end of Sec. IV A.

Qualitative interpretation of the L-edge white lines of Rh, Pd, and Ag. As discussed above, the absorption features at the near-edge region can readily be compared with the calculated density of states. At the L_{II} and L_{III} edges, the initial state, which has an angular momentum $l=1$, probes the unoccupied states of $s(l=0)$ and $d(l=2)$ character (the $\Delta l=+1$ transition is, by far, more intense). There exist many theoretical band-structure calculations[48–50] which give similar density-of-states results for these metals. Here we employ the systematic study by MGW.[46,51] Their band-structure results for these elements and the corresponding partial density of states are shown in Fig. 4 up to 10 eV above the Fermi level. Two apparent features are noteworthy regarding the property of the metal bands upon going from Rh to Ag: First, the top of the d band moves from above (in the case of Rh) to below the Fermi level (in the case of Ag) as the d band becomes filled; second, the drop in energy (increasing binding energy) of the d band is accompanied by band narrowing. This can be easily seen from the partial density of states. The increase in binding energy of the occupied d band and the accompanying band narrowing for these elements have already been borne out in photoemission studies by Smith *et al.*[47] The near-edge results, on the other hand, enable us to study the unoccupied d states above the Fermi level. These states are very important in compound formation, upon which charge redistribution takes place.

Comparing Figs. 2–4, one can immediately assign the observed features within the first 10 eV above the edge (E_F). In Rh metal the white lines at the L_{II} and L_{III} edges are assigned to $2p\rightarrow 4d$ transitions. The observation that the tail of the white line extends to several electron volts above E_0 (E_F) is consistent with a high density d states at the Fermi level, followed by a rather broad and smooth distribution. The same assignment is made for the white lines at the Pd L_{II} and L_{III} edges. For Rh and Pd all these L_{II},L_{III} white lines should rise at the Fermi level, and the point of inflection of the rising edge is pinned as the Fermi level. The positions of the labeled peaks are given in Table I.

Based on the electronic configuration and band calculations, it is expected that the width and intensity of the white lines for Rh, when normalized to the edge jump, should be greater than those for Pd. This is observed in Figs. 2 and 3. In the case of Ag, the d bands are essentially full and no white line is observed at the $L_{II,III}$ edge, consistent with the calculation. This result clearly shows that the L-edge white line is very sensitive to the occupancy of the d states. Three weak peaks are observable at 2.0, 5.2, and 8.8 eV above the threshold in the Ag L_{III} edge, where the $p\rightarrow d$ white line would have appeared if the d band of Ag had remained partially unoccupied. These peaks are assigned to $2p\rightarrow s$ band transitions. The calculated DOS exhibits high density at these positions.

The L_I near-edge structures above the Fermi level are similar for Rh and Pd (Figs. 2 and 3). This is expected

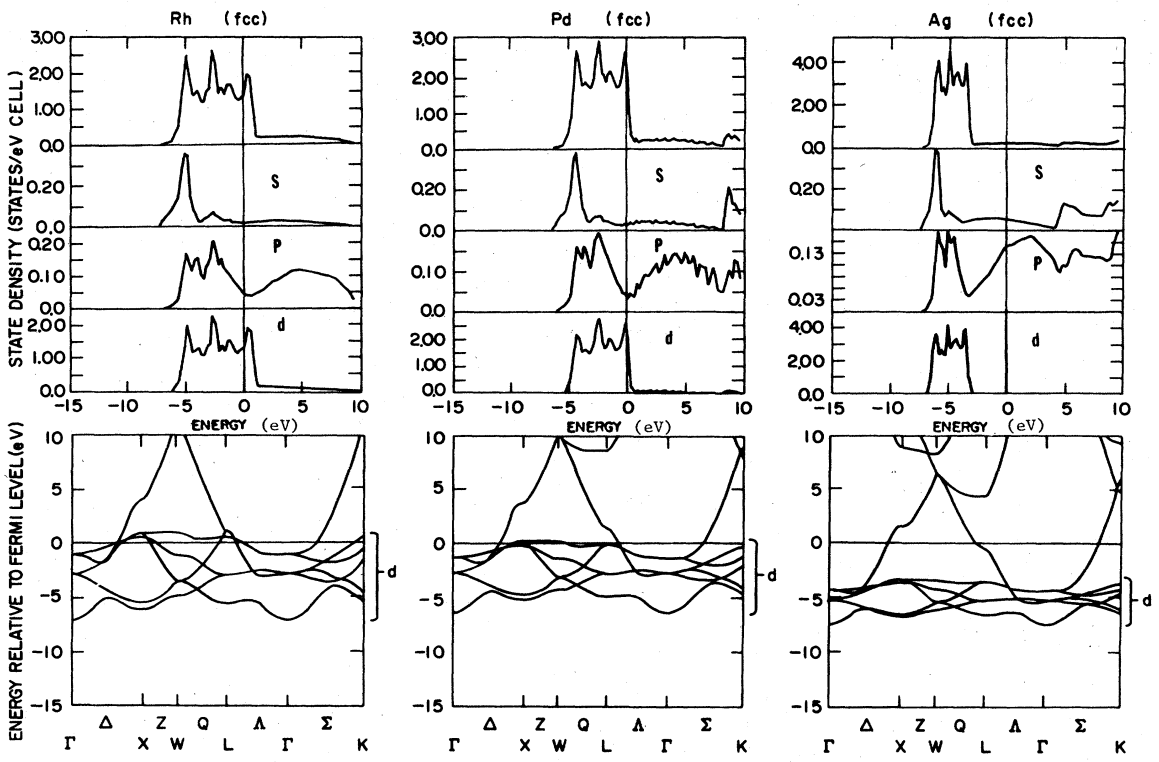

FIG. 4. Density-of-states calculation by Moruzzi, Gelatt, and Williams using an augmented-spherical-wave technique (Refs. 46–51) for Rh, Pd, and Ag; the width of the *d* band is marked on the right-hand side of the band-structure diagram; the energy is in electron volts and the zero position is the Fermi level.

from the calculated distribution of the partial density of states. Both metals exhibit no white lines, but do exhibit a broad structure at ~5 eV above the Fermi level. This feature can be tentatively assigned to a $2s \rightarrow p$ state transition, which is expected based on Fig. 4. The intensity and width of this feature are consistent with the delocalized nature of the *p*-band states. The Ag L_I-edge spectrum shows slightly different features; which are shown in Fig. 5, together with previously reported Ag *K*-edge results based on experiment and theory.[17] The first peak is only ~2 eV above the Fermi level, followed by a broad peak that rises at ~5 eV and peaks at ~10 eV above the threshold (these peaks are clearly identified in the derivative spectrum). The glitch at 3800 eV is due to the monochromator. Again, this observation is expected on the basis of Fig. 4, where the *p* density of states peaks at 2 eV, 6 eV, and begins to rise at 9 eV. Overall, we have seen the qualitative agreement between experiment and ground-state band calculations to be remarkable within the first 10 eV of the Fermi level. It thus appears that, for these metallic elements, the *L*-edge XANES can be described very well in terms of the ground-state band calculation of

TABLE I. Observed (Obs.) and calculated (Calc.) positions (in eV) of the XANES maxima relative to the Fermi level [peak 1 corresponds to the white line in the L_{III} spectra of Rh and Pd, and to the Fermi level in the Ag L_{III} spectrum. Estimated uncertainty is ±0.2 eV. The calculated values are provided by Müller (private communication)] in the L_{III} edge of Rh, Pd, and Ag.

Peak position	Rh Obs.	Rh Calc.	Rh Δ[a]	Pd Obs.	Pd Calc.	Pd Δ[a]	Ag Obs.	Ag Calc.	Ag Δ[a]	Assignment[b]
1	0	0	0	0	0	0	2.0	1.0	1.9	*d* (*s*)
2	10.2	9.4	0.6	8.6	8.5	0.1	5.2	4.0	1.2	
3	14.7	14.5	0.2	14.4	13.0	1.4	9.5[c]	7.8	1.7	*pd*
4	21.8	21.6	0.2	23.4	22.5	0.9	18.5	17.4	1.1	
5	29.0	28.7	0.2	30.0	29.1	0.9	26.5	25.1	1.4	*df*
6	38.7	38.6	0.1	38.7	38.1	0.6	34.8	33.4	1.4	*f*
7	53.0	51.7	1.3	51.4	51.0	0.4	45.5	44.6	0.9	*df*

[a]Difference between observed and calculated results (Δ = Obs. − Calc).

[b]According to Ref. 17 (see text); the assignment in the parentheses is for Ag.

[c]Peak 3 in the Ag spectrum has more structure than a single peak; this is taken as the midpoint of the structure (a sharper feature occurs at 8.8 eV).

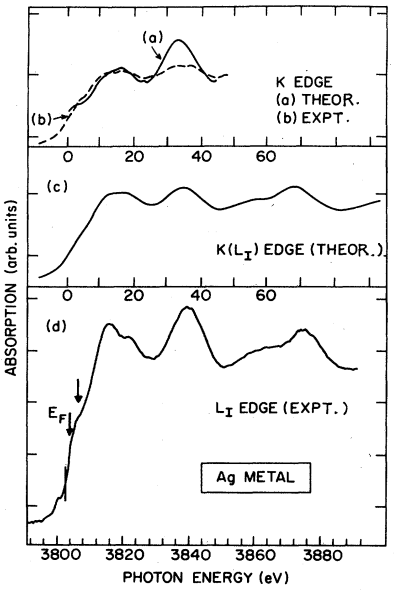

FIG. 5. L_{I}- and K-edge spectra of Ag metal from theory and experiment: (a) experiment by Müller *et al.*; (b) theory by Durham *et al.* (Ref. 15); (c) theory by Müller *et al.* (Ref. 17); (d) L_{I}-edge experiment (this work), with the arrows showing the positions of the first two weak absorptions, which are clearly identifiable in the derivative spectrum; the glitch below E_F is due to the monochromator.

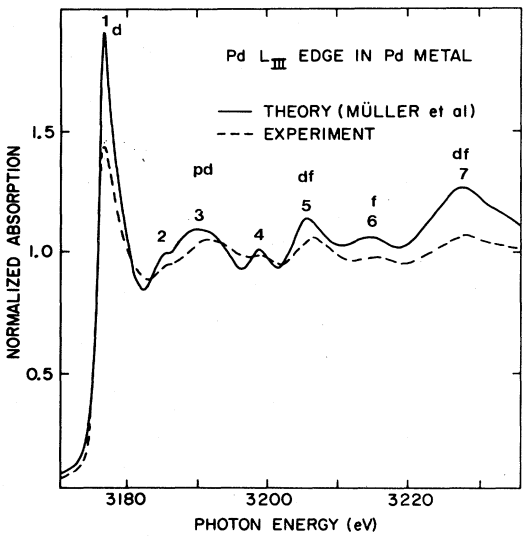

FIG. 6. Comparison of experimental and calculated L_{III}-edge XANES of Pd metal. The resonance maxima are given in Table I.

the distribution of the density of states of different angular momentum. It has been noted that f orbitals on neighboring atoms may give a p-type symmetry to the local density of states.[15,17] This, however, becomes important only at higher energies and is discussed further in the following section.

Quantitative comparison of experimental $L_{II,III}$ spectra of Rh, Pd, and Ag with theoretical spectra based on single-particle calculation. A detailed comparison of the oscillatory behavior of the experimental L_{III} spectrum with the theoretical result[17] is shown in Fig. 6 for Pd. Both spectra are normalized to the smooth (atomic) edge jump. The theoretical spectrum already takes into account the lifetime effect of the core hole and the final-state photon-energy-dependent contribution.[17] The calculated L_{II} edge should look exactly the same as the L_{III} spectra, according to the one-electron calculation. The only difference is a scale factor in the atomic factor in the absorption. This leads to $\mu(L_{\mathrm{II}})=0.47\mu(L_{\mathrm{III}})$ in palladium metal, where $\mu(L_{\mathrm{II}})$ and $\mu(L_{\mathrm{III}})$ are the absorption coefficients for the L_{II} and L_{III} edges, respectively. A scale factor of 0.5 is observed experimentally for the smooth atomic background edge jump in all three metals, but the relative intensities of the observed and the calculated white lines, which depend somewhat on the distribution of the $d_{5/2}$ and $d_{3/2}$ character resulting from spin-orbit interaction of the d states, do not agree very well with theory. This is not surprising because spin-orbit interaction was neglected in these calculations. One important comparison is the relative positions of the maxima of the oscillating absorption coefficient determined theoretically and experimentally. Qualitatively, the resemblance of the experimental and theoretical results is clearly evident.

According to the calculations,[17] the absorption spectrum can be factorized into a smooth atomic term and a solid-state term. The latter has a rapidly varying energy dependence and is responsible for all the observable oscillations in the near-edge region of the absorption spectrum. There are several important features derived from the solid-state term in the theoretical Pd L_{III} spectrum: (a) There is a narrow non-free-electron-like $4f$ band (begins to come in at $\sim$25 eV above the Fermi level) resulting from the centrifugal term in the effective potential for the partial waves of palladium; the $4f$ band moves down towards the Fermi level across the period and becomes a narrow f-band bound state at the Fermi level for the rare-earth metals;[52] (b) hybridization involving the narrow $4d$ and $4f$ bands, and other nl bands, results in that the partial densities of states with lower angular momentum become suppressed and pushed away from the narrow band, and that other partial densities of states exhibit a replica of $4d$ and $4f$ character, the latter coming about from the projection of the tail of the orbitals centered in adjacent sites onto all values of angular momentum of the central atom. These states are all labeled in Fig. 6, where the white line is of primarily $4d$ character: $5d$ begins to come in at higher energy and interacts with the $4f$. pd, df, etc. are the hybrid states.

The oscillatory behavior of the spectrum of Pd matches peak for peak with theory, including weak features up to 60 eV above the threshold. Similar situations are also seen in the case of Rh and Ag. Detailed assignments can now be made. The first peak in Fig. 6 again can be assigned to a $2p\rightarrow 4d$ band transition. Peaks 2—4 arise from transitions to hybridization states involving primarily $5p$ and some $4d$ character, peak 3 being the primary p state. The $4f$ band interacts strongly with the $5d$ band, resulting in peaks 5—7, where peaks 5 and 7 have some $5d$ character. All these agreements clearly support the density-of-states picture; that is, the absorption coefficient

is directly related to the projected density of states ($l=2$). The above analysis and the difference in peak positions of all the L_{III} edges in Rh, Pd, and Ag are listed in Table I. From Table I and Figs. 2–4, one finds that the same L_{III}-edge pattern is observed upon going from Rh to Pd to Ag. It is interesting to note that all the resonances move to lower energy at higher atomic number. This is consistent with the theory which predicts that the resonance states across the $4d$ period move towards lower energy upon filling of the electronic states. The observed peak positions are expected to occur at slightly higher photon energy than that calculated by Müller *et al.*, due to the effect of electron—core-hole interaction in the final state.[52] This shift is expected to be more important at higher energies and results in a relaxation shift in the photoelectron spectrum in photoemission studies. Another interesting observation is the energy difference between the observed and calculated resonance peaks. This difference, which increases from Rh to Pd to Ag, is attributed to a more dominant initial-state effect resulting from a less effective screening by the d electrons in the case of Ag.

The relative intensities of the observed and the calculated white lines of Rh, Pd, and Ag are given in Table II. The intensities are normalized to the edge jump and are measured by the height of the peak with respect to the extrapolated background of the pre-edge. The area of the peaks, although theoretically more meaningful, is difficult to obtain due to experimental resolution and photon-energy-dependent broadening. The results (Table II) show that theory and experimental results agree very well in the atomic part of the absorption coefficient (ratio of the edge jump is given in the second column). The intensity of the white lines observed in the L_{II},L_{III} spectra of Rh and Pd are only in qualitative agreement with theory (the last two columns). This discrepancy is partly due to experimental resolution broadening in the data and partly due to the spin-orbit interaction, which is not dealt with in the calculation.

Spin-orbit interaction characteristics and the relative intensity of the L_{II} and L_{III} white lines. The perhaps most interesting observation (Table II) is that while the $I(L_{III})/I(L_{II})$ white-line intensity ratio for Rh is in good agreement with the statistical ratio, the same ratio deviates significantly in the case of Pd. This discrepancy can be regarded as a consequence of spin-orbit effects.[29] According to dipole-transition selection rules, $2p_{1/2}$ and $2p_{3/2}$ electrons probe $4d_{3/2}$ and $4d_{5/2}$ states according to $\Delta j=0,\pm1$. Thus these relative white-line intensities provide not only information about the number of unoccupied d states, but also about total-angular-momentum characteristics. Since the selection rule forbids transition from a core $p_{1/2}$ state to a $d_{5/2}$ valence state, the observed ratio is expected to deviate from the 2-to-1 ratio, depending on the distribution of the $d_{5/2}$ and $d_{3/2}$ character at the Fermi level. From the energetic point of view, states of $d_{3/2}$ character should lie lower in energy (higher binding energy), and the observed intensity ratio $I(L_{III})/I(L_{II})$ is expected to be $\geq 2/1$ in general. In the case of the third-row transition metals, the spin-orbit effect is comparable to banding; thus the deviation from 2/1 should be most obvious compared with its first- and second-row counterparts. It is expected that the distribution of $d_{3/2}$ and $d_{5/2}$ character should be nearly the same when the spin-orbit coupling is small and there are a large number of unoccupied states at the Fermi level (that is, in metals in which the d band is far from filled), while in metals in which the d band is nearly full, the unoccupied $d_{5/2}$:$d_{3/2}$ ratio is expected to deviate from the statistical ratio markedly. It has been found that the intensity ratio of the Ta L_{III} and L_{II} white lines in Ta metal (s^1d^4 configuration) is close to the statistical ratio,[20] while that of the Pt L_{III} and L_{II} white lines is much greater than the statistical ratio[16,19] (in fact, the white line is only observed in the L_{III} edge in Pt metal). The latter observation has been attributed to the almost exclusive $d_{5/2}$ character at the Pt Fermi level.[16,19,53] The situation for the second-row noble metals is not as drastic as in the case of the third-row noble metals because the spin-orbit interaction in Pd and Ag is ($\sim$0.2 eV) about an order of magnitude smaller than that of the corresponding third-row noble metals and acts as a perturbation to the banding. Significant deviation in the $I(L_{III})/I(L_{II})$ ratio is not expected, except in the case where the d vacancy at the Fermi level is small (it has been calculated that Pd has $\sim$0.36 holes per atom in its d band).[54] Experimentally, the deviation is indeed observed to be more significant in Pd as compared with Rh (Table II), and this difference is attributed to a relatively high density of unoccupied states of $d_{5/2}$ character at the Fermi level of the Pd metal.

TABLE II. $L_{II,III}$ white-line (WL) and edge-jump (EJ) intensities of Rh, Pd, and Ag. $[I(\mathrm{EJ})]_{L_{III}}$, etc. is the smooth (atomic) edge-jump intensity; $[I(\mathrm{WL})]_{L_{III}}$, etc. is the white-line intensity. Since Ag does not exhibit a white line, the first peak is used for the measurement; the height of the peak is used to measure the intensity. The calculated ratios are based on theoretical spectra (Ref. 17). Uncertainty is ±0.1. EJ is often taken as the difference between pre-edge absorption and that of the midpoint between the maxima and minima of the first few oscillations.

	$[I(\mathrm{EJ})]_{L_{III}}/[I(\mathrm{EJ})]_{L_{II}}$		$[I(\mathrm{WL})]_{L_{III}}/[I(\mathrm{WL})]_{L_{II}}$	
Element	Calc.	Obs.	Calc.	Obs.
Rh	2	~2	~2	1.9
Pd	2	~2	2.09	2.7
Ag	2	~2	~2	2.0

The total width of the d band from L_{III}-edge XANES and photoemission. The width of the $L_{II,III}$ white lines in Rh, Pd, and Ag are discussed here in detail. We recall that there are several factors that determine the profile of the white line; they are the lifetime of the core hole, the experimental resolution, the dipole-transition matrix element, and the distribution of the density of states (as measured by the bandwidth). For Pd and Rh metals, the first three factors can be assumed to be the same for all the $L_{II,III}$ edges to a first approximation, since the binding energies do not differ significantly (a few percent). Given this assumption, the observed white-line widths can be attributed to the distribution of the density of states of the unoccupied d band at the Fermi level of the metals.

Before we discuss the linewidth, it is worthwhile to dis-

TABLE III. Observed and calculated d-band widths (Γ) for Rh, Pd, and Ag from XPS and L_{III}-edge white lines.

	Γ observed (eV)				Γ calculated (eV)[c]		
	XPS[a]	XANES[b] I	XANES[b] II	Total	Occupied	Unoccupied	Total
Rh	6.7	3.5	1.0	7.7	6.3	0.8	7.1
Pd	6.2	3	0.4	6.6	5.3	0.3	5.6
Ag	4.3	~0	~0	4.3	3.9	~0	3.9

[a]Taken from Ref. 47 using a procedure analogous to that of Fuggle *et al.* [Phys. Rev. B **27**, 2179 (1983)].

[b]Column I is taken as twice of the half-width of the rising Lorentzian edge (±0.2 eV); and, in column II, core-hole widths (Ref. 17) of 2.0 and 2.1 eV for Rh and Pd, respectively, and a resolution of ~0.5 eV, have been subtracted from column I.

[c]From Refs. 26 and 47, all the band calculations give widths within a few tenths of an electron volt.

cuss the profile of these white lines. Wei and Lytle[20] have analyzed the line shape of the L-edge white line of Ta metal in detail, and have found that the white-line—absorption envelope is slightly better described with a Fano-type function than with a Lorentzian line shape, while Horsley[30] has used the scheme of a Lorentzian and an arctangent function to describe the $L_{II,III}$ white lines in a series of Pt and Ir compounds. These analyses are appropriate only when the density of states is narrow. For our purposes any of the above approaches would give a reasonable and self-consistent set of widths for comparison. Here we have taken an empirical approach by measuring the half-width of the rising Lorentzian edge. After subtraction of the lifetime and instrumental contribution, the tentatively derived DOS widths of the d band are obtained. These are given in Table III. It can be clearly seen from Table III (column I under XANES) that the observed DOS width of Rh is already greater than that of Pd by 0.5 eV, despite the fact that the lifetime and resolution contribution to the observed width for the Pd edge is greater than that for Rh. This observation is in semiquantitative agreement with band calculations which show that there should be a wider distribution of unoccupied d states just above the Fermi level in Rh metal (Fig. 4 and Table III) than in Pd metal. These widths, derived from L_{III}-edge XANES, together with the bandwidth given by photoemission, now present a complete description of the (occupied and unoccupied) d bands in these noble metals. The semiquantitative agreement shown in Table III, in turn, strongly suggests that L-edge white lines in these elements indeed probe the distribution of the unoccupied d states.

L_I- and K-edge spectra of Rh, Pd, and Ag: A comparison of the observed XANES with theory. Figure 7 shows the detailed comparison of the XANES portion of the L_I- and K-edge spectra of Pd with theory.[17] A similar comparison for Ag is already shown in Fig. 5. Agreement between experiment and theory is strikingly good, although the theoretical positions of the maxima in the absorption spectrum are slightly lower in energy than those observed. This discrepancy is most likely due to core-hole—final-state interaction (relaxation), and has been discussed earlier in connection with the $L_{II,III}$ edge.

The theoretical spectra for the L_I and K edges of Pd are identical, as expected, except that the atomic factor and the final-state lifetime are different. The observed L_I- and K-edge spectra [Figs. 7(a) and 7(b)] are identical at the EXAFS region. The L_I oscillations are sharper as a result of better overall resolution. The most noticeable differences between the L_I- and K-edge spectra of Pd (also Rh) are the intensity and position of the second peak, which is ~17 eV above the Fermi level. This peak arises from $5p$-$4d$ hybridization states with considerable $5p$ character. This difference is probably due to the difference in the overlap between $2s \rightarrow 5p$ and $1s \rightarrow 5p$ transitions, as well as contributions from the L_{II} edge.

The resolution of the XANES data presented here is considerably better than that of the K-edge results reported previously, and it is therefore desirable to reexamine

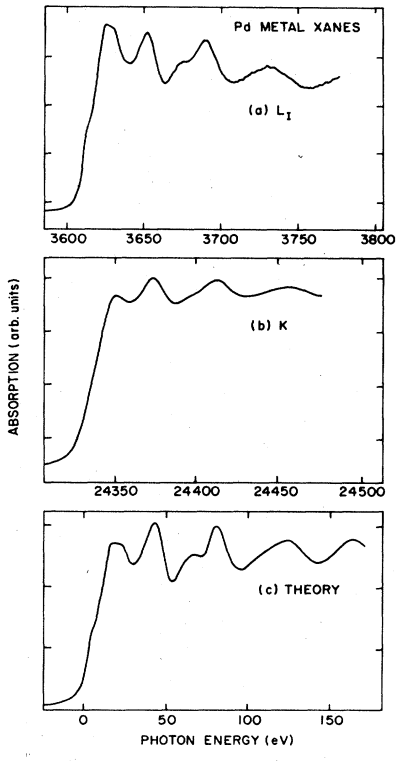

FIG. 7. Detailed comparison of L_I- and K-edge XANES of Pd metal (theory and experiment): (a) and (b) are spectra from this work, and (c) is theory from Ref. 17 for Pd L_I edge.

the earlier interpretation[17,35] of the K-edge XANES of Rh, Pd, and Ag metal using the L_I-edge results. In the interpretation of the earlier work,[17,35] the three essential features observed at ~5, ~20, and ~40 eV above the Fermi level are attributed to transitions from the core level to projected density of $l=1$ states arising from $4d$, $5p$, and $4f$ characters, respectively. They find that while the $5p$ band contributes directly from orbitals with $l=1$, the $4d$ and $4f$ orbitals also contribute via orbitals centered at the sites adjacent to the excited atom (a solid-state effect). The valleys between the three peaks are due to suppressions of hybridization that occur when the $5p$ band overlap with the d and $4f$ bands. A detailed comparison of our data is shown in Fig. 8. The relevant parameters are summarized in Table IV. From Fig. 8 and Table IV we observe (a) the position of peak d shifts to lower photon energy (relative to E_F) from Rh to Pd to Ag; (b) the position of peak $5p$ follows a different trend—it shifts very little at Pd and has the lowest energy at Ag—and the peak is actually split, with the splitting being the largest in Ag (7.9 eV) [these results were not observed in previous K-edge spectra (a broadening was observed), due to poor resolution, and are consistent with the calculated DOS which predicts splitting in this region due to hybridization]; (c) peak f is relatively narrow when compared with peak p—it stays at about the same position in Rh and Pd, but shifts to lower energy in Ag and broadens only slightly due to final-state effects and resolution. These observations confirm most of the earlier interpretations,[35] except that the so-called peak d does not seem to disappear at the Ag L_I edge, although the Ag $L_{II,III}$-edge results and band theory show that there is very little d character at the Fermi level of Ag. The d peak at the Ag L_I edge, of which the intensity is no less, if not more intense, than that observed in Rh or in Pd, must arise from states with considerable p character that become involved in dp hybridization. A closer look at the Ag K-edge results (Fig. 5) reveals that the calculation of Durham *et al.*[15] using a three-shell (43-atom) cluster and multiple-scattering considerations also reproduces the XANES feature of Ag K edge, but the splitting of the $5p$ peak is not apparent.

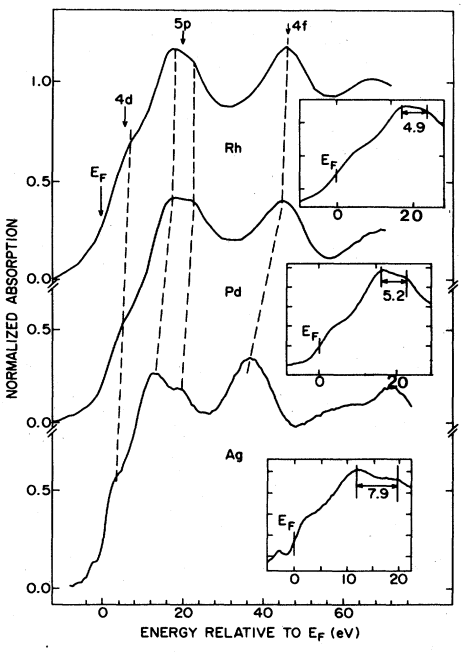

FIG. 8. L_I-edge spectra of Rh, Pd, and Ag, where $5p$ (pd hybrid state with primarily p character) and $4f$ are similar to the pd and f assignments used in the L_{III}-edge study.

TABLE IV. Assignments of absorption maxima (relative to the Fermi level) of L_I-edge XANES of Rh, Pd, and Ag metals.

Metal	Peak position (eV)	Assignment[a]
Rh	7.3	$2s\rightarrow 4d,dp$
	17.0, 21.9	$2s\rightarrow 5p,pd$
	45.9	$2s\rightarrow 4f$
	68.0	$2s\rightarrow df$ or EXAFS
Pd	5.4	$2s\rightarrow 4d,dp$
	16.9, 22.1	$2s\rightarrow 5p,pd$
	44.0	$2s\rightarrow 4f$
	66.0	$2s\rightarrow df$ or EXAFS
Ag	3.8	$2s\rightarrow 4d,dp$
	11.9, 19.8	$2s\rightarrow 5p,pd$
	36.0	$2s\rightarrow 4f$
	60.0	$2s\rightarrow df$ or EXAFS

[a] dp or df denote hybridization states (Refs. 17 and 18) involving $4d,5p$ and $5d,4f$ states, respectively; these hybrid states have the same meaning as those discussed in the assignment of the L_{III} edge.

Another interesting aspect of the theoretical and experimental comparison of the L_I (K-edge) spectrum is that it leads to the question of how the XANES region and the EXAFS region should be defined and analyzed. It has become common practice to classify the first (50—60)-eV region in the vicinity of the threshold as the XANES region, and to analyze the data in terms of absorption intensity; on the other hand, in standard EXAFS analysis, data with k values >3 Å^{-1} (~ 30 eV $>E_0$) are commonly used to extract structural information according to Eq. (6). Here we explore the consequences of analyzing the theoretical spectrum with the EXAFS approach, since the calculated spectrum extends to 160 eV above the threshold.

Figure 9 presents the Fourier-transform analysis of the calculated spectrum, as well as the observed spectra at a large range of k values. The oscillating curves in Fig. 9 are the normalized $\chi(k)k^2$ EXAFS functions, where panel (a) is the full length of the K-edge spectrum (up to $K=15$ Å^{-1}), and panels (b), (c), and (d) are the EXAFS functions of the K-edge, L_I-edge, and theoretical XANES data, respectively (k from 2 to 7 Å^{-1}). The corresponding Fourier transforms are shown in panels (e)—(h). Several interesting features can be noted from these figures. First, the theoretical spectrum panel (d), shows almost identical patterns as the observed K-edge [panel (b)] and L_I-edge [panel (c)] spectra, except that the separation between the

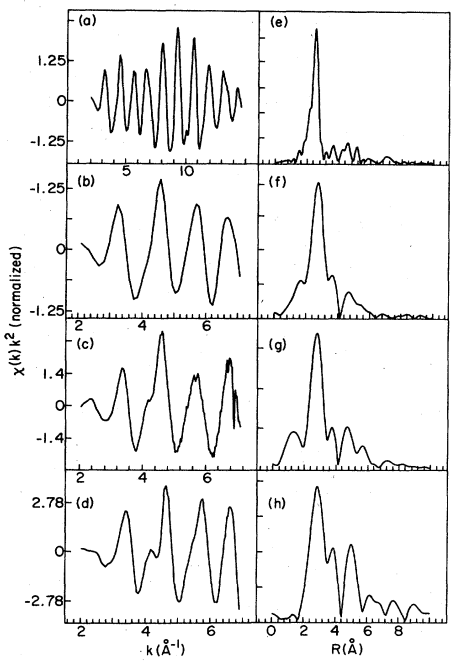

FIG. 9. Fourier analysis of the EXAFS $[\chi(k)k^2]$ of Pd: (a) K-edge full length, (b) K-edge XANES, (c) L_{I}-edge XANES, (d) L_{I}(theory) XANES, and (e)—(h) are corresponding Fourier transforms.

EXAFS maxima of the theoretical spectrum becomes slightly smaller at high k as a result of greater mismatches in peak positions. This is also reflected in the Fourier transform which peaks at a slightly larger distance ($+0.1$ Å) in R space than those derived in the experimental data. The exact position of the peak in R space is irrelevant for this discussion due to the limited length and other multidistance complications, as it is evident from Fig. 9(a) that the envelope corresponding to the nearest neighbor comes in at higher k values. Second, the EXAFS amplitude, which is of great importance in accurate structural analysis, exhibits the following order: theory $> L_{\mathrm{I}} > K$ (theoretical spectrum has zero experimental resolution and zero Debye-Waller factor); this observation clearly shows the effect of overall resolution in EXAFS amplitude analysis.

B. L-edge spectra and the distribution of density of states in In and Sn metals

The L-edge spectra and their corresponding derivatives for In and Sn metals are shown in Figs. 10 and 11, respectively. It is immediately apparent that they are distinctly different from those of Pd and Rh in that there is no white line at the L_{II} and L_{III} edges, but there is a white line at the L_{I} edge. This turn around of the appearance of white lines upon going from Rh, Pd, and Ag to In and Sn can be understood qualitatively on the basis of their electronic configurations and electron energy-band considerations. Let us first consider the d states. In the second transition period, the $4d$ shell of the atoms is being filled as we go from left to right across the period until the d shell is completely filled in the case of Ag(d^{10}). In metals, it is the d band that becomes filled in a similar manner, except that hybridization among the valence states $5s$, $5p$, and $4d$ pushes some d character above the Fermi level and the d band also becomes practically filled at Ag. As one leaves the transition period and moves into the main-group elements (metalloids or polyvalent metals) such as Cd, In, and Sn, the $4d$ states are completely filled and grow deeper and deeper in energy (becoming more corelike). The unoccupied states in the vicinity of the Fermi level are primarily of s and p character. The maximum of the distribution of the $5d$ states are still well above the vacuum level in these elements and the total

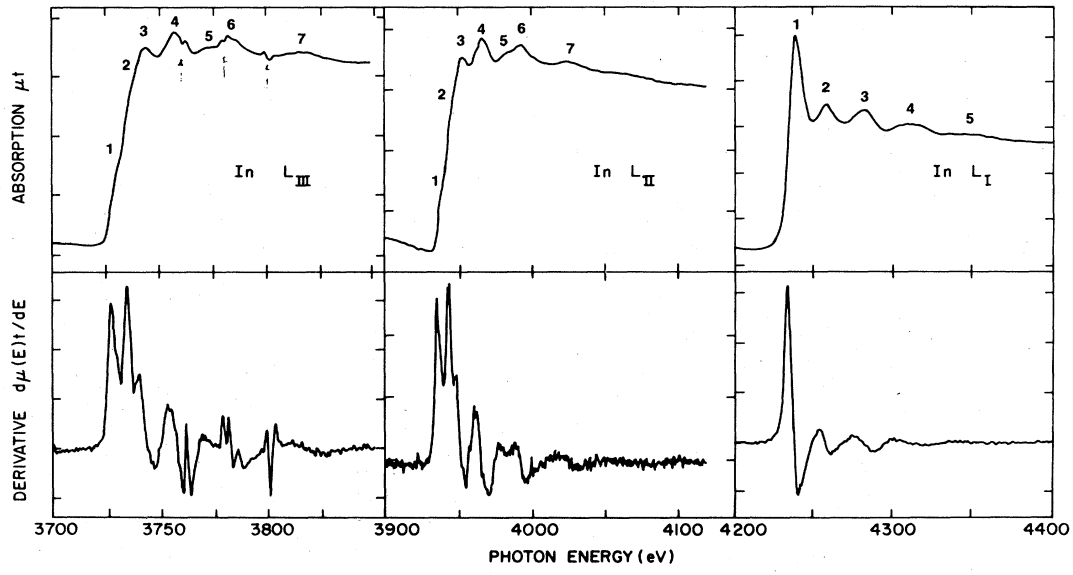

FIG. 10. L-edge spectra of In metal and corresponding first derivatives. Monochromator glitches are marked with arrows.

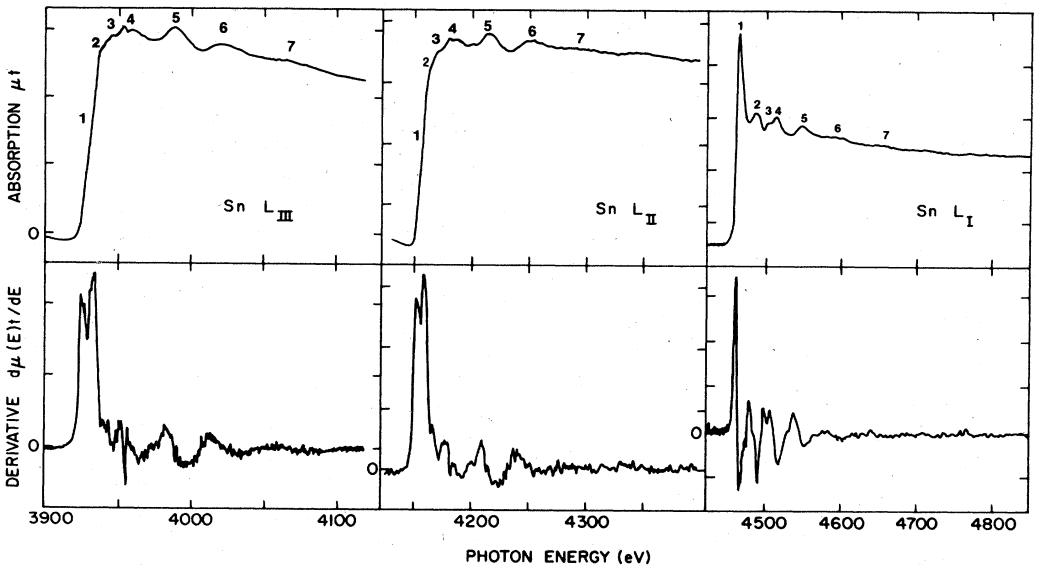

FIG. 11. L-edge spectra of Sn metal and corresponding first derivatives.

drop (collapse[54]) of these levels does not occur until the element achieves a rare-gas-like configuration. This is discussed further in a forthcoming paper in connection with the Cs^+ and I^- EXAFS. For the $P_{3/2,1/2}$ core levels in the polyvalent metals, the states in the vicinity of the Fermi level that they can couple to are states with $l=0$ and 2. These are primarily states with s character which are often more delocalized, and have a relatively weak oscillator strength and a small amount of $5d$ character. The $5d$ character in the vicinity of the Fermi level increases as the $5p$ band becomes filled. Intense white lines are, therefore, not expected to be observable at the $L_{II,III}$ edges of these elements. The valence p states, on the other hand, remain largely unoccupied despite s-p hybridization (sp^2 in In and sp^3 in Sn). These p states are slightly more localized than their counterparts in noble metals, where s and p states are conductionlike. Since the p states in these main-group metals are far from being filled, there is a high density of these states just above the Fermi level. It is expected that the L_I edge of In and Sn should exhibit white lines arising from $2s \rightarrow 5p$ transitions. In addition, the f band that develops as a unique feature[17] (Figs. 6 and 8) in the $4d$-transition-metal series begins to move towards the Fermi level and hybridizes with all the s, p, and d states to produce more fine structures. Experimentally, all the aforementioned expectations are observed.

Absorption features at the first 15 eV above the edge threshold can be compared with the partial density of states derived from band calculations[46] of MGW (who use lattices different from the real lattice of these metals), bearing in mind that the lattice structures do not greatly influence the DOS of the metal. Their DOS plots for the first 10 eV above the Fermi level are shown, in Fig. 12, to assist the qualitative interpretation. The L_{II} and L_{III} spectra of In are nearly identical. They both exhibit a three-peak feature (two small shoulders) just above the Fermi level. These shoulders are clearly observable in the derivative spectrum. These peaks may be assigned to $2p \rightarrow 5s$ transitions according to the DOS calculations for both fcc and bcc lattices. These calculations show that there are unoccupied states of s character just above the Fermi level, where the densities of states of d character are practically negligible, although the presence of two peaks is not indicated in these calculations. This discrepancy is probably due to the lowering of symmetry in the real lattice (tetragonal distortion), the projection of higher-momentum states as in the case of Rh, Pd, and Ag, as well as a partial collapse of the $5d$ and $4f$ states upon core-hole creation, or due to multielectron effects. A similar situation is observed in the L_{II} and L_{III} edges of Sn (of which the local environment is also tetragonal), except that the second shoulder in Sn is more intense than

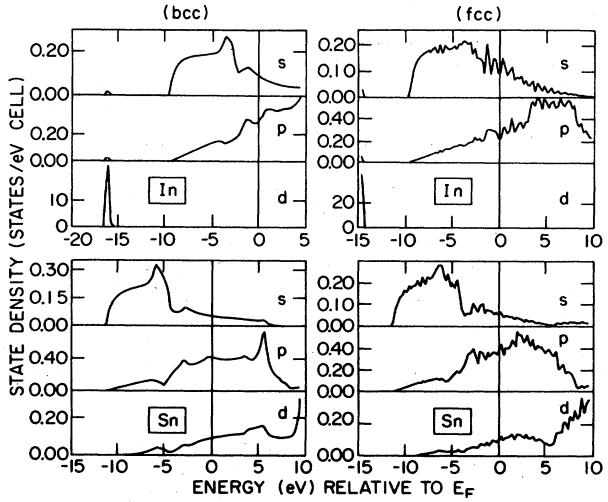

FIG. 12. DOS of In and Sn calculated by MGW (Ref. 46) using bcc and fcc lattice parameters; note that the $5d$ characters begin to show up in the vicinity of the Fermi level in Sn.

TABLE V. Peak positions in the L_{III} and L_I near-edge spectra of In and Sn.

Edge	Peak no.	Peak position (eV) relative to E_F In	Assignment	Sn	Assignment[a]
L_{III}	1	3.8	*sp*	3.9	*sp,pd*
	2	10.8		13.0	
	3	17.7	*pd,df*	21.1	*pd,df*
	4	32.3	*f*	32.6	*f*
	5	49.6	*df*	64.8	*df*
	6	59.2		96.1	EXAFS
	7	90.8	EXAFS	141.6	
L_I	1	2.6	*sp*	4.4	*sp,pd*
	2	23.7	*f*	23.4	*f*
	3	47.9	*df*	37.8	*df*
	4	75.8	EXAFS	46.6	*df* or EXAFS
	5	113.4		54.0	
	6			89.4	EXAFS
	7			131.2	

[a]Tentative, based on Pd results; *d* refers to 5*d* (see text).

that in the case of In. This is not expected based on unoccupied *s* states alone because the *s* states are being filled much faster than the *p* states. There must be some 5*d* character that begins to drop into the vicinity of the Fermi level in the case of Sn. Both bcc and fcc DOS's show that this is the case. The observation of the intense white line in the L_I edge in both metals is consistent with the presence of a high density of *p* states above the Fermi level. The peak positions and white-line parameters for In and Sn are shown in Tables V and VI. The peak parameters are about the same for both In and Sn white lines, but are different from those of the $p \rightarrow d$ transition in noble metals in that these $2s \rightarrow p$ transitions are more symmetric.

Quantitative interpretation of the XANES of In and Sn extending to higher energy is not feasible at the present time since theoretical calculation of the *L*-edge spectra of these metals is not available. It can be noted, however, that the $L_{II,III}$ edges exhibit structures that are similar to those of Pd with the 5*p* states (labeled *pd* in the calculation of Müller *et al.*) shifted down to the Fermi level. The difference is due to the fact that as soon as the 4*d* level becomes corelike in main-group metals, it becomes inactive in the hybridization that was previously responsible for the complex Pd $L_{II,III}$ edge. Semiquantitative assignments can still be made for the In and Sn spectra based on the Pd calculation with the following considerations: First, the narrow 4*f* band that moves closer to the Fermi should be responsible for some weak features in the first-50-eV region. Second, the 5*d* band should begin to develop and hybridize with the 4*f* band. Third, the characteristics of the development of the higher bands are preserved across the period. Finally, these high-energy bands are assumed to be only slightly sensitive to lattice parameters. Tentative assignments using conventions identical to those used in the assignment of the Pd L_{III} and L_I spectra are listed in Table V. The slight difference between In and Sn in the assignment in Table V is due to the 5*d* band, which begins to have an influence at the Fermi level in Sn. The *sp* and *p* bands described in Table V are equivalent to the *pd* band discussed in Fig. 8 for Pd, and the rest of the assignment has the same meaning as those described earlier. By comparing the L_I edge in Fig. 10 with Fig. 8, we can argue that peaks 5*p* and 4*f* in Fig. 8 move down and become peaks 1 and 2 in Fig. 10, respectively; that is, that the partially filled *p* band is now at the Fermi level. It is interesting to note that the Cd L_I-edge XANES is more Ag-like (no L_I-edge white line) than In-like, indicating that the 5*p* maximum in Cd is still a distance from the Fermi level. The movement of these states are less discernible in the L_{II},L_{III} edges due to hybridization and the involvement of $l=0$ and $l=2$ final states. The general oscillatory behavior of the absorption coefficient in the region starting at ~50 eV above the threshold is consistent with what is expected based on EXAFS theory.

The width of the white line is again of some interest. As we move across the main-group metals, two changes to the *p* bands should occur. One is the filling of the *p* band and the other is the narrowing of the *p* band. The experimental width of the In L_I white line is the same as that of Sn, despite a small increase in lifetime broadening and slightly poorer energy resolution for Sn (Table VI). This observation again demonstrates the sensitivity of the *L*-edge XANES technique in probing the distribution of the density of states.

TABLE VI. L_I white line parameters of In and Sn.

	Position (relative to E_F)	Width[a]	Intensity[b]
In	2.6	4 (7)	1.53
Sn	4.4	4 (7)	1.62

[a]Half-width of the rising edge; the value in the parentheses is the width between the first maximum and minimum in the derivative spectrum.

[b]The height of the white line relative to the smooth edge jump.

V. SUMMARY AND CONCLUSIONS

What emerges from the above analysis is a picture in which the development of the unoccupied density of states above the Fermi level in the $4d$ period follows the same trend as that predicted by band calculation and observed by PES techniques. The most noticeable development seen in this study is the sensitivity of white lines toward chemical changes. Going from Rh to Pd to Ag, the total L_{III},L_{II} white-line intensity decreases and the L_{III},L_{II} white lines are not observed in the case of Ag and Cd, in which the d band is filled. This observation correlates qualitatively with ground-state band calculations[46] of MGW and semiquantitatively with the theoretical spectrum calculated by Müller, Jensen, and Wilkins.[17] The relative intensity ratio of the L_{III},L_{II} white lines is also reported and subtle difference in this ratio for elements across the period is attributed to the nonstatistical distribution of density states of unoccupied $d_{5/2}$ and $d_{3/2}$ character for bands that are nearly full. The sensitivity of the XANES technique in probing electronic properties of compounds is illustrated with the Pd, $PdAl_3$, and $PdCl_2$ series in paper II.

In the main-group metals In and Sn, in contrast to the noble metals, no white line is observed in the $L_{II,III}$ edge, but an intense white line is seen at the L_I edge. This observation is interpreted on the basis of the relative positions (distribution of the DOS) of the s, p, d and f bands across the polyvalent ($5p$) period. Detailed assignment of the near-edge structure of main-group metals awaits more elaborate procedures.

Interesting systematics concerning the behavior of the XANES features can be established. This is illustrated in Fig. 13, where the peak positions of two near-edge absorption features are plotted against the metallic elements across the period. The f and pd correlations are obtained from the L_I-edge measurements, where the assignments were based on the calculation of Müller *et al.*[17] The position of these peaks should, to a great extent, characterize the movement of the unoccupied f and p bands, respectively, across the period. It can be seen that both the f and pd band drop considerably once the $4d$ band is filled and the pd band becomes more p-like and drops to the vicinity of the Fermi level at In (the Cd L_I-edge spectrum is Ag-like and a sharp spike is not seen until In is reached).

Several remarks concerning the future development of the analysis of L-edge absorption may be made here. First, electron correlation effects are not included in the analysis presented here. The inclusion of this effect would give rise to satellite peaks above the corresponding absorption. Such additional satellites are not clearly seen in the case of the noble metals (single-particle calculation accounts for all the peaks observed), although satellites have been observed in Pd and Pd alloys at 6—10 eV above the core-level binding energy in XPS experiments,[55] and more prominent satellite features have been observed in the Mn K edge of $MnCl_2$.[37] Second, in the case of In and Sn, however, energy-loss processes resulting in plasmon satellites have been seen in XPS studies.[56] Such processes would also give satellites at the near-edge structure if the process is intra-atomic. The exact nature of the absorption peaks in the L-edge spectra of In and Sn is yet to be determined. Finally, it is very desirable to introduce a proper potential to deal with the presence of the core hole undergoing adiabatic and sudden excitation and to develop a unified description of near-edge structure.

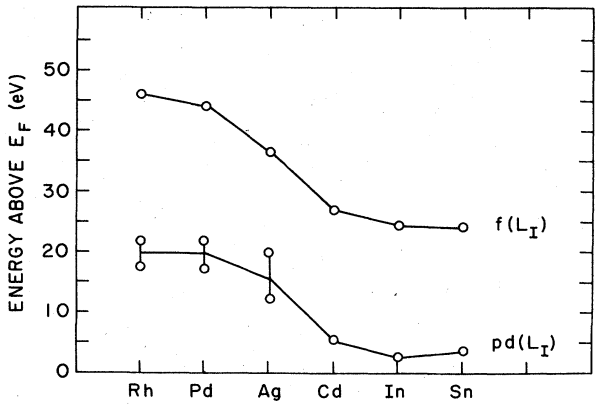

FIG. 13. L-edge—absorption systematics (from Rh to Sn: the position of some characteristic resonances relative to the Fermi level is plotted against the elements; the f and pd correlations correspond to the behavior of $pd(5p)$ and $f(4f)$ peak as assigned in Figs. 8, 10, and 11. The Cd values are from unpublished results. The splitting observed in Fig. 8 is also shown.

ACKNOWLEDGMENTS

I would like to thank J. E. Müller, J. W. Wilkins, Dr. V. Moruzzi, A. R. Williams, and R. E. Waston for making their results available prior to publication and for discussions, and J. Davenport, M. Newton, J. Stöhr, and N. Sutin for discussions. I am indebted to W. Kunmann and E. Ritter for the preparation of the metal and alloy samples. This research was carried out at Brookhaven National Laboratory under contract with the U.S. Department of Energy and supported by its Office of Basic Energy Sciences. EXAFS data were collected at SSRL, which is supported by the National Science Foundation through the Division of Material Research and the National Institute of Health through the Biotechnology Resource Program in the Division of Research Resources, and the U.S. Department of Energy, through its Office of Basic Energy Sciences.

---

[1] *EXAFS and Near Edge Structure,* edited by A. Bianconi, L. Incoccia, and S. Stipcich (Springer, New York, 1983).

[2] Edge jump usually occurs when the photon energy is slightly less than the binding energy of the core level. This is because the bound-state—to—bound-state transition takes place at photon energies less than the ionization energy of the core level.

[3] H. Winick and A. Bienenstock, Annu. Rev. Nucl. Part. Sci. 28,

33 (1979).
[4]*Synchrotron Radiation,* edited by C. Kunz (Springer, New York, 1979).
[5]R. E. Watson and M. L. Perlman, Science **199**, 1295 (1978).
[6]P. Eisenberger and B. Kincaid, Science **200**, 1441 (1978).
[7]At the current state of development, XAS is conveniently divided into x-ray-absorption near-edge structure (XANES) and extended x-ray-absorption fine structure (EXAFS) (see Ref. 1). General consideration of x-ray techniques can be found in *X-ray Spectroscopy,* edited by L. V. Azaroff (McGraw-Hill, New York, 1977).
[8]*Synchrotron Radiation Research,* edited by H. Winick and S. Donaich (Plenum, London, 1980).
[9]R. G. Schulman, T. Yafet, P. Eisenberger, and W. E. Blumberg, Proc. Natl. Acad. Sci. (USA) **73**, 1384 (1976).
[10]G. D. Mahan, in *Solid State Physics,* edited by H. Ehrenreich, F. Seitz, and D. Turnbull (Academic, New York, 1974), Vol. 29, p. 75.
[11]F. C. Brown, in *Solid State Physics,* edited by H. Ehrenreich, F. Seitz, and D. Turnbull (Academic, New York, 1974), Vol. 29, p. 1.
[12]P. A. Lee, P. Citrin, P. Eisenberger, and B. Kincaid, Rev. Mod. Phys. **53**, 769 (1981), and references cited therein.
[13]J. Stöhr and J. Jaeger, Phys. Rev. B **26**, 4111 (1982).
[14]B. K. Teo and P. A. Lee, J. Am. Chem. Soc. **101**, 2915 (1979).
[15]P. J. Durham, J. B. Pendry, and C. H. Hodges, Solid State Commun. **38**, 159 (1981).
[16]M. Brown, R. E. Peierls, and E. A. Stern, Phys. Rev. B **15**, 738 (1977).
[17]J. E. Müller, O. Jepsen, O. K. Andersen, and J. W. Wilkins, Phys. Rev. Lett. **40**, 720 (1978); J. E. Müller, O. Jepsen, and J. W. Wilkins, Solid State Commun. **42**, 365 (1982); J. E. Müller and J. W. Wilkins, Phys. Rev. B **29**, 4331 (1984).
[18]J. E. Müller and W. L. Schaich, Phys. Rev. B **27**, 6489 (1983).
[19]L. F. Mattheiss and R. E. Dietz, Phys. Rev. B **22**, 1663 (1980).
[20]P. S. P. Wei and F. W. Lytle, Phys. Rev. B **19**, 676 (1979).
[21]F. W. Lytle, P. S. P. Wei, R. B. Greegor, G. H. Via, and J. H. Sinfelt, J. Chem. Phys. **70**, 4849 (1979).
[22]L. A. Grunes, R. D. Leapman, C. N. Wilkes, R. Hoffman, and A. B. Kunz, Phys. Rev. B **25**, 7157 (1982).
[23]L. A. Grunes, Phys. Rev. B **27**, 2111 (1983).
[24]F. W. Kutzler, C. R. Natoli, D. K. Misemer, S. Donaich, and K. O. Hodgson, J. Chem. Phys. **73**, 3275 (1980).
[25]A. Bianconi, Phys. Rev. B **26**, 2741 (1982).
[26]A. Balzarotti, F. Comin, L. Incoccia, M. Piacentini, S. Mobilio, and A. Savoia, Solid State Commun. **35**, 145 (1980).
[27]T. K. Sham, J. Am. Chem. Soc. **105**, 2269 (1983).
[28]T. K. Sham, J. Chem. Phys. **79**, 1116 (1983).
[29]T. K. Sham, in Abstract in Americal Chemical Society Meeting, Atlanta, Georgia, April 1980 (unpublished), and Ref. 1.
[30]J. A. Horsley, J. Chem. Phys. **76**, 1451 (1982).
[31]R. Haensel, G. Keitel, N. Kosuch, U. Nielsen, and P. Schreiber, J. Phys. (Paris) Colloq. **32**, C4-236 (1971).
[32]J. Hastings and P. Eisenberger, in Abstract to the Fifth International Conference on Vacuum Ultraviolet Radiation Physics, Montpellier, France, 1977 (unpublished).
[33]J. L. Dehmer and D. Dill, J. Chem. Phys. **65**, 5327 (1977); P. M. Dittman, D. Dill, and J. L. Dehmer (unpublished).
[34]T. A. Carlson, M. O. Krause, and W. E. Moddeman, J. Phys. (Paris) Colloq. **32**, C4-76 (1971); F. Wuilleumeir, *ibid.* **32**, C4-88 (1982).
[35]V. O. Kostroun, R. W. Fairchild, C. A. Kukkonen, and J. W. Wilkins, Phys. Rev. B **13**, 3268 (1976).
[36]A. Balzarotti, M. De Cresenzi, and L. Inoccia, Phys. Rev. B **25**, 6349 (1982).
[37]E. A. Stern, Phys. Rev. Lett. **49**, 1353 (1982).
[38]L. M. Mattheiss, Phys. Rev. **133**, A1399 (1964).
[39]G. Wendin, in *Structure and Bonding* (Springer, New York, 1981), Vol. 45.
[40]U. Gelius, J. Electron Spectrosc. Relat. Phenom. **5**, 985 (1974).
[41]S. Svensson, N. Mårtenssen, E. Basilier, P. Å. Malmquist, U. Gelius, and K. Siegbahn, Phys. Scr. **14**, 141 (1976).
[42]S. P. Kowalczyk, L. Ley, R. L. Martin, F. R. McFreeley, and D. S. Shirley, Faraday Discuss. Chem. Soc. **60**, 7 (1975).
[43]T. K. Sham and G. Wendin, Phys. Rev. Lett. **44**, 817 (1980).
[44]G. M. Bancroft, P. A. Malmquist, S. Svensson, E. Basilier, U. Gelius, and K. Siegbahn, Inorg. Chem. **17**, 1595 (1978).
[45]E. A. Stern and K. Kim, Phys. Rev. B **23**, 3781 (1981).
[46]V. L. Moruzzi, C. D. Gelatt, and A. R. Williams (private communication).
[47]N. V. Smith, G. K. Wertheim, S. Hüfner, and M. M. Traum, Phys. Rev. B **10**, 3197 (1974).
[48]N. E. Christensen, Phys. Rev. B **14**, 3446 (1976).
[49]R. Lässer and N. V. Smith, Phys. Rev. B **25**, 806 (1982).
[50]A. H. MacDonald, J. M. Daams, S. H. Vosko, and D. D. Koelling, Phys. Rev. B **23**, 6377 (1981); **25**, 713 (1982).
[51]A. R. Williams, J. Kübler, and C. D. Gelatt, Jr., Phys. Rev. B **19**, 6094 (1979).
[52]J. E. Müller (private communication); G. Materlik, J. E. Müller, and J. W. Wilkins, Phys. Rev. Lett. **50**, 267.
[53]This interpretation was first suggested by Mott. See N. F. Mott, Proc. R. Soc. London **62**, 416 (1949), and U. Cauchois and N. F. Mott. Philos. Mag. **40**, 1260 (1949).
[54]J. P. Connerade, J. Phys. B **11**, L381 (1978).
[55]B. Chandesris, G. Krill, G. Maire, J. Leconte, and J. Petroff, Solid State Commun. **37**, 187 (1981).
[56]R. A. Pollak, L. Ley, F. R. McFeeley, S. P. Kowalczyk, and D. A. Shirley, J. Electron Spectrosc. Relat. Phenom. **3**, 381 (1974).